# Aharonov–Bohm oscillations in carbon nanotubes

**Adrian Bachtold*, Christoph Strunk*, Jean-Paul Salvetat†, Jean-Marc Bonard†, Laszló Forró†, Thomas Nussbaumer* & Christian Schönenberger***

** Institut für Physik, Universität Basel, Klingelbergstrasse 82, CH-4056 Basel, Switzerland*

*† Institut de Génie Atomique, École Polytechnique Fédérale de Lausanne, CH-1015 Lausanne, Switzerland*

**When electrons pass through a cylindrical electrical conductor aligned in a magnetic field, their wave-like nature manifests itself as a periodic oscillation in the electrical resistance as a function of the enclosed magnetic flux[1]. This phenomenon reflects the dependence of the phase of the electron wave on the magnetic field, known as the Aharonov–Bohm effect[2], which causes a phase difference, and hence interference, between partial waves encircling the conductor in opposite directions. Such oscillations have been observed in micrometre-sized thin-walled metallic cylinders[3–5] and lithographically fabricated rings[6–8]. Carbon nanotubes[9,10] are composed of individual graphene sheets rolled into seamless hollow cylinders with diameters ranging from 1 nm to about 20 nm. They are able to act as conducting molecular wires[11–18], making them ideally suited for the investigation of quantum interference at the single-molecule level caused by the Aharonov–Bohm effect. Here we report magnetoresistance measurements on individual multi-walled nanotubes, which display pronounced resistance oscillations as a function of magnetic flux. We find that the oscillations are in good agreement with theoretical predictions for the Aharonov–Bohm effect in a hollow conductor with a diameter equal to that of the outermost shell of the nanotubes. In some nanotubes we also observe shorter-period oscillations, which might result from anisotropic electron currents caused by defects in the nanotube lattice.**

In a diffusive and thin-walled metallic cylinder, a prominent periodic quantum correction to the resistance arises from the interference of closed electron trajectories that encircle the cylinder once. The phase difference $\Delta\phi$ between each such trajectory $\Gamma$ and the time-reversed counter-propagating trajectory $\Gamma'$ (Fig. 1a) is solely determined by the magnetic flux $\Phi$ enclosed: $\Delta\phi = 2\pi(2e/h)\Phi$, where $e$ and $h$ are the electron charge and Planck's constant, respectively. Consequently, the electrical resistance has an oscillating contribution with period $h/2e$, known as the Altshuler–Aronov–Spivak (AAS) effect[1]. For zero magnetic flux, these interference terms add up constructively, increasing electron backscattering and thereby the electrical resistance, an effect known as weak localization[19]. For a thin metallic film in a perpendicular magnetic field, the weak-localization resistance correction monotonically disappears in higher fields (negative magnetoresistance, MR). In contrast, for a cylinder in a parallel magnetic field, weak localization is periodically modulated with a magnetic-field period given by $\Delta B = (h/2e)/r^2\pi$, where $r$ is the radius of the cylinder.

We have carried out electric-transport measurements on multi-walled carbon nanotubes (MWNTs) composed of multiple coaxial graphene cylinders, in a magnetic field parallel to the axis of the nanotubes. An example is shown in Fig. 1b. Coulomb blockade can strongly affect electrical transport in small structures, and we therefore use samples containing only a single contacted nanotube with low contact resistances (that is, not exceeding a few kilohms). Although this approach will not completely exclude Coulomb blockade effects, the different measurements and control experiments carried out indicate that Coulomb blockade is, at most, of minor importance. For example, we have never observed that cooling leads to an increase in the resistance of a nanotube towards an isolating state, as would be expected for Coulomb blockade, and current–voltage characteristics were checked to be linear to at least 10 mV. We have also performed control experiments using an additional gate electrode. For electrostatic gating fields of up to $10^8$ V m$^{-1}$, we observed resistance changes not exceeding 10%. Although the changes depend weakly on the electric field, we have not been able to gate the nanotube into an insulating state, as would occur if Coulomb blockade were important.

Figure 2 shows the measured electrical resistance (solid curves) of a MWNT as a function of magnetic field $B$ for different temperatures. A large modulation of the resistance (~30%) is observed, comparable in size to the quantum resistance $h/2e^2$. Starting from $B = 0$, the resistance decreases with increasing field. Previous studies in perpendicular magnetic fields observed, a similar decrease in MR which could be interpreted within the framework of weak localization[11,17]. It thus seems reasonable to assume that the same physics is responsible for the resistance change seen here. At higher magnetic fields, a second resistance peak develops at $\pm 8.8$ T. This second peak is assigned to the reappearance of enhanced backscattering due to the AAS effect. As expected, a similar peak is not observed in perpendicular fields.

To provide further evidence for the resistance oscillations constituting AAS effects, we compare our measurements with theoretical predictions for the AAS effect in cylinders[1,4]. We first determine the

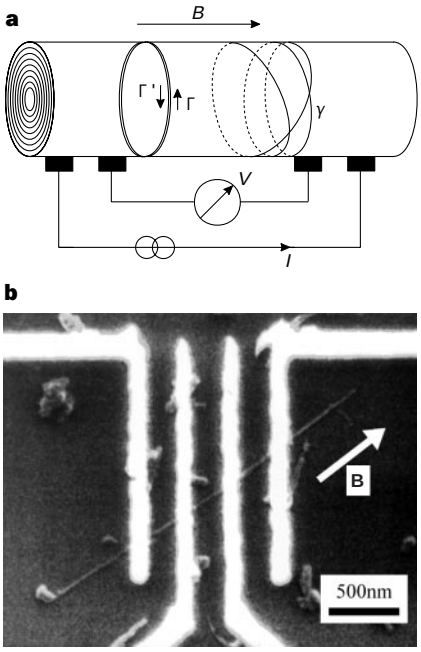


**Figure 1** A single multi-walled carbon nanotube electrically contacted with four electrodes. **a**, Diagram of a multi-walled nanotube (MWNT), which is composed of a series of coaxial graphene cylinders. The electrical resistances of single MWNTs are measured via four electrical contacts (imposed current $I$ and measured voltage $V$) in a magnetic field $B$ which is aligned parallel to the tube axis to within a few degrees. A periodic magnetoresistance is expected to originate from quantum interference of counter-propagating closed diffusive electron trajectories, like those denoted by $\Gamma$ and $\Gamma'$ or $\gamma$. **b**, Scanning-electron microscopy (SEM) image of a MWNT contacted by four Au fingers; the direction of **B** is shown by a white arrow. The MWNTs are produced by arc-discharge evaporation[27]. After purification[28], they are adsorbed from a dispersion in chloroform onto an oxidized Si wafer. An electrode structure, consisting of four Au fingers which are 70 nm thick, ~100 nm wide, 2 μm long, and separated by 350 nm (centre-to-centre), is then patterned onto the nanotubes using electron-beam lithography. As a SEM image can only give a qualitative estimate for the diameter of the nanotube, atomic force microscopy is used to determine the diameter of an electrically measured MWNT.

effective (that is, the mean current-carrying) cylinder radius $r_e$ from the peak position at a magnetic field of 8.8 T. As this field ought to correspond to a magnetic flux of $h/2e$ threading the cross-section $\pi r_e^2$, a radius of $r_e = 8.6 \pm 0.1$ nm is inferred. This value is in excellent agreement with the outer radius $r_0 = 8 \pm 0.8$ nm of the nanotube as determined by atomic force microscopy and not, as one might have expected, with the mean radius of all graphene cylinders of this MWNT (expected to be $\lesssim$5 nm).

For comparison with theory, we first consider a single graphene cylinder with known radius $r_e$. Then, three parameters appear in the AAS theory: the misalignment angle $\Theta$ between the magnetic field direction relative to the cylinder axis, the length $L$ of the current-carrying part of the cylinder between the contacts, and the temperature-dependent phase-coherence length $l_\phi$. We note that a value of $\Theta$ of a few degrees can account for the observed reduced amplitude of the resistance peaks at $\pm$8.8 T (ref. 4). Matching the theory to the measurement at $T = 1.8$ K, we obtain $l_\phi = 54$ nm, $L = 170$ nm and $\Theta = 4.4°$. These values of $\Theta$ and $L$ agree well with the geometry of this sample. Keeping $\Theta$ and $L$ constant, a similar procedure is applied to the other MR curves. As illustrated in Fig. 2, we find good agreement between theory (dotted lines) and experiment (solid lines). This agreement is obtained while assuming that only one graphene cylinder contributes to the conductance. We may relax this assumption by considering a set of concentric cylinders which carry the electrical current equally. Under the constraints given by the measured outer diameter (for possible radii $r$) and the distance between contacts (for $L$), we find that at most two outer shells can contribute; this is much less than the number of shells that make up an actual MWNT (in our case, ~20 are expected).

We therefore conclude that quantum-interference corrections to the resistance can account for the measured MR, if and only if the electrical current is assumed to flow in one (or two) of the outermost shells. This finding may be understood as follows: by virtue of the fabrication technique, contact is made to the outer surface of the nanotube, so that current is injected into the outermost conducting graphene cylinder. As nanotubes can be conducting or insulating[20–24], the outermost conducting tube may be followed by an insulating one, restricting the conduction to one cylinder. It is also possible that the anisotropy of the conductivity, which resembles graphite[25], is enough to keep the current confined to one cylinder, in particular at low temperatures where inter-shell hopping is suppressed. Owing to the small current-carrying cross-section, a remarkably low resistivity is obtained. We estimate this resistivity to be $\lesssim 10\,\mu\Omega$ cm at room temperature, which is comparable to that of metals with good conductivity.

In addition to the MR shown in Fig. 2, we have also observed an oscillatory feature on several other MWNTs (we believe that this latter feature has not been previously observed). Figure 3 shows such a measurement for two temperatures for a nanotube of outer radius $r_0 = 6.5 \pm 0.5$ nm determined by atomic force microscopy. The most striking and immediately visible difference from the previously mentioned sample is a superimposed short-period oscillation (see arrows). In agreement with the MR of the previous sample, the resistance (neglecting the rapid oscillation) at first decreases with increasing magnetic field. Then, it develops a minimum at ~9 T and increases again, possibly towards a second maximum, which is beyond the experimental field range and is expected at ~18 T from the measured size of the tube. The linear

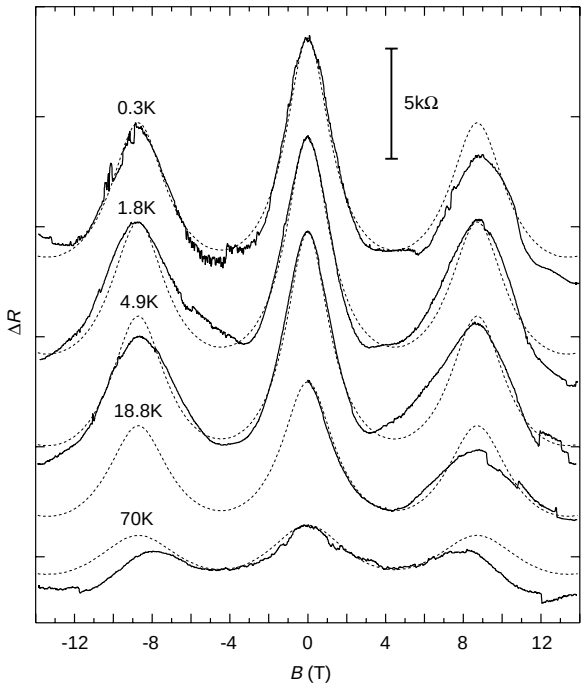


**Figure 2** Magnetoresistance $R(B)$ at five different temperatures $T$ measured for a MWNT in a parallel magnetic field $B$ (solid curves). The dotted curves correspond to theoretical predictions for the quantum correction to the resistance of a thin-walled cylindrical conductor using the parameters: $r_e = 8.6$ nm, $\theta = 4.4°$ and $L = 170$ nm for the effective cylinder radius, the angle between magnetic field and cylinder axis, and the length of the cylinder between the electric contacts, respectively. All curves are vertically offset for clarity. At zero field the absolute values for the resistances are (kΩ): 30.6, 30.1, 29.8, 25 and 21.4 from top to bottom ($T = 0.3, \ldots, 70$ K). Non-reproducible temporal resistance jumps are observed in the experiment, possibly caused by temporal changes in the electric contacts, defects or impurities in the nanotubes.

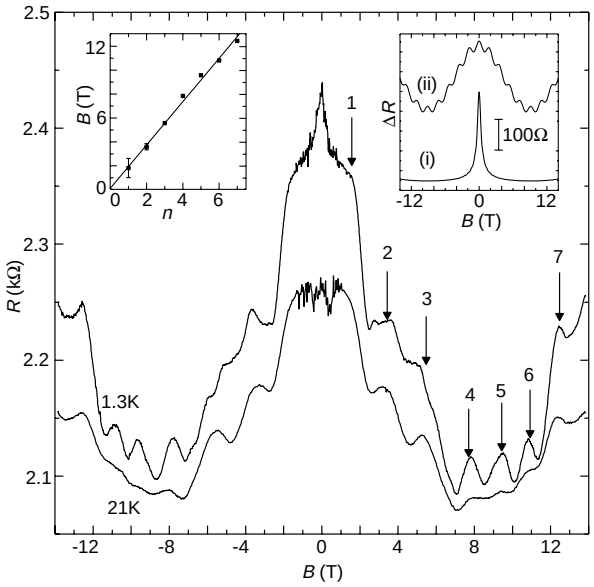


**Figure 3** As Fig. 2 but for two different temperatures $T$ on another MWNT. The general decrease of the resistance from 0 T to ~9 T, and the subsequent increase to a possible second maximum (beyond the magnetic-field range of the experiment), is assigned to the fundamental oscillation of the AAS effect. In addition, a superimposed oscillation with a much smaller period is clearly visible. Positions of maxima in resistance for this oscillation are labelled by arrows and plotted in the left inset, which shows that the oscillation is periodic with period $\Delta B_{fast} = 1.8$ T. The peak positions agree for both temperatures. This oscillation is interpreted to originate from electron interference of preferentially selected higher-order loops which wind several times around the nanotube (see also Fig. 1a). Right inset, theoretically predicted MR for (i) the 'full' AAS effect (that is, adding up corrections from loops with all winding numbers) and (ii) the case when only trajectories with winding number 1 and 10 are considered. For both cases, we require the magnitude of the resistance correction to match the experimental data. The strong temporal resistance fluctuations, which appear near zero field, are not yet understood, but disappear for larger fields $|B| \gtrsim 1.5$ T.

dependence of the peak positions of the short-period oscillation on magnetic field (Fig. 3 left inset) demonstrates that a periodic oscillation is observed with period $\Delta B_{\mathrm{fast}} = 1.8\,\mathrm{T}$. $\Delta B_{\mathrm{fast}}$ cannot correspond to the fundamental $h/2e$ period of the AAS effect, as this condition would require a cylinder with an effective radius of $r_e = 19\,\mathrm{nm}$, which is significantly larger than the outer radius for this nanotube. As the two peaks denoted by 3 and 7 appear approximately symmetrical with respect to the gross-minimum of the MR curve, the minimum is assigned to coincide with peak number 5. The fundamental AAS period then comprises $n = 10$ 'fast' oscillations.

Being convinced about the assignment for the fundamental AAS period, we ask where the 'fast' magneto-oscillation may come from. Closed electron trajectories that encircle the tube once (winding number 1) give rise to the fundamental magnetic flux-period $h/2e$. Trajectories with a larger winding number $n > 1$ (see, for example, the $n = 3$ loop denoted by $\gamma$ in Fig. 1a) contribute to the resistance with an oscillating term given by $K_0(n2\pi r/l_\phi)\cos(2\pi n\Phi/(h/2e))$; the amplitude is determined by the modified Bessel function $K_0(x)$ (refs 1, 4). Though such a contribution has a flux-period which is $n$-times smaller than $h/2e$, the present theory cannot account for the experimental result. The reason is that the sum over all terms $n = 1, \ldots, \infty$ of this Fourier series describes a smooth periodic function with period $h/2e$. Higher-order oscillations, as observed, can only show up if trajectories with specific winding numbers are preferentially selected. In order to allow a qualitative comparison, we display in the right inset of Fig. 3 the theoretical resistance dependence for two cases: (i) the contributions from all winding numbers are summed according to theory, (ii) only the $n = 1$ and $n = 10$ terms are retained. The latter resembles the measurement much more closely. From the condition that the amplitude of the $n = 1$ and $n = 10$ terms should agree with the measurement, the phase-coherence length is estimated to be $l_\phi \approx 250\,\mathrm{nm}$, which is much larger (by a factor of 6.5) than the circumference $2\pi r_e$, in contrast to the previous example for which $l_\phi \approx 2\pi r_e$. This difference may be the reason why specific higher-order terms do not appear in the measurement of Fig. 2. We note that taking only two terms with distinct winding numbers to contribute to the resistance correction is justified as a first guess, but certainly oversimplifies the problem. In general, there is a distribution of weights for the higher-order terms which is specific for each nanotube, and is observed to differ from the AAS prediction.

Although we have an understanding of the long-period oscillations, the appearance of higher-order terms is at present unexplained. One possibility is that the short-period oscillations are due to chiral currents in strained nanotubes[26]. Chirality is a well established structural property of carbon nanotubes. In principle, graphitic tubules have isotropic conductivity; but when they are mechanically stretched owing to the interaction with the substrate, or owing to thermal contracting, the 'honeycomb' lattice can be distorted resulting in anisotropic, chiral current. Chirality can select particular winding numbers which give the higher-order term superimposed on the long-period oscillations observed in Fig. 3. In an MWNT the chirality can change from layer to layer, and the period of short oscillations can vary from tube to tube and from sample to sample. This fine structure in the AAS oscillations is closely related to the special structure of the carbon nanotubes, and further experimental and theoretical studies are needed for its detailed understanding. □

Received 25 August; accepted 8 December 1998.


1. Altshuler, B. L., Aronov, A. G. & Spivak, B. Z. The Aharonov–Bohm effect in disordered conductors. *Pis'ma Zh. Eksp. Teor. Fiz.* **33,** 101–103 (1981) [*JETP Lett.* **33,** 94–97 (1981)].
2. Aharonov, Y. & Bohm, D. Significance of electromagnetic potentials in the quantum theory. *Phys. Rev.* **115,** 485–491 (1959).
3. Sharvin, D. Y. & Sharvin, Y. V. Magnetic-flux quantization in a cylindrical film of a normal metal. *Pis'ma Zh. Eksp. Teor. Fiz.* **34,** 285–288 (1981) [*JETP Lett.* **34,** 272–275 (1982)].
4. Aronov, A. G. & Sharvin, Y. V. Magnetic-flux effects in disordered conductors. *Rev. Mod. Phys.* **59,** 755–779 (1987).
5. Gijs, M., Van Haesendonck, C. & Bruynseraede, Y. Resistance oscillations and electron localization in cylindrical Mg films. *Phys. Rev. Lett.* **52,** 2069–2072 (1984).
6. Pannetier, B., Chaussy, J., Rammal, R. & Gandit, P. Magnetic flux quantization in the weak-localization regime of a nonsuperconducting metal. *Phys. Rev. Lett.* **53,** 718–721 (1984).
7. Webb, R., Washburn, S., Umbach, C. & Laibowitz, D. C. Observation of $h/e$ Aharonov–Bohm oscillations in normal-metal rings. *Phys. Rev. Lett.* **54,** 2696–2699 (1985).
8. Chandrasekhar, V., Rooks, M. J., Wind, S. & Prober, D. E. Observation of Aharonov–Bohm electron interference effect with period $h/e$ and $h/2e$ in individual micro-sized, normal-metal rings. *Phys. Rev. Lett.* **55,** 1610–1613 (1985).
9. Ijima, S. Helical microtubules of graphitic carbon. *Nature* **354,** 56–58 (1991).
10. Dresselhaus, M. S., Dresselhaus, G. & Eklund, P. C. *Science of Fullerenes and Carbon Nanotubes* (Academic, San Diego, 1986).
11. Langer, L. *et al.* Quantum transport in multiwalled carbon nanotubes. *Phys. Rev. Lett.* **76,** 479–482 (1996).
12. Dai, H., Wong, E. W. & Lieber, C. M. Probing electrical transport in nanomaterials: conductivity of individual carbon nanotubes. *Science* **272,** 523–526 (1996).
13. Ebbesen, T. W. *et al.* Electrical conductivity of individual carbon nanotubes. *Nature* **382,** 54–56 (1996).
14. Tans, S. J. *et al.* Individual single-wall carbon nanotubes as quantum wires. *Nature* **386,** 474–477 (1997).
15. Bockrath, M. *et al.* Single-electron transport in ropes of carbon nanotubes. *Science* **275,** 1922–1925 (1997).
16. Bachtold, A. *et al.* Contacting carbon nanotubes selectively with low-ohmic contacts for four-probe electric measurements. *Appl. Phys. Lett.* **73,** 274–276 (1998).
17. Bachtold, A., Strunk, C., Schönenberger, C., Salvetat, J.-P. & Forró, L. in *Proc. XIIth Int. Winterschool on Electronic Properties of Novel Materials* (eds Kuzmany, H., Fink, J., Mehring, M. & Roth, S.) 65–68 (AIP, New York, 1998).
18. Frank, S., Poncharal, P., Wang, Z. L. & Heer, W. A. Carbon nanotube quantum resistors. *Science* **280,** 1744–1746 (1998).
19. Begmann, G. Weak localizations in thin films. *Phys. Rep.* **107,** 1–56 (1984).
20. Hamada, N., Sawada, D.-I. & Oshiyama, A. New one-dimensional conductors: graphite microtubules. *Phys. Rev. Lett.* **68,** 1579–1581 (1992).
21. Saito, R., Fujita, M., Dresselhaus, G. & Dresselhaus, M. S. Electronic structure of chiral graphene tubules. *Appl. Phys. Lett.* **60,** 2204–2206 (1992).
22. Mintmire, J. W., Dunlap, B. I. & White, C. T. Are fullerene tubules metallic? *Phys. Rev. Lett.* **68,** 631–634 (1992).
23. Wildöer, J. W. G., Venema, L. C., Rinzler, A. G., Smalley, R. E. & Dekker, C. Electronic structure of atomically resolved carbon nanotubes. *Nature* **391,** 59–62 (1998).
24. Odom, T. W., Huang, J.-L., Kim, P. & Lieber, C. M. Atomic structure and electronic properties of single-walled carbon nanotubes. *Nature* **391,** 62–64 (1998).
25. Wallace, P. R. The band theory of graphite. *Phys. Rev.* **71,** 622–634 (1947).
26. Miyamoto, Y. Mechanically stretched carbon nanotubes: Induction of chiral current. *Phys. Rev. B* **54,** R11149–R11152 (1996).
27. Ebbesen, T. W. & Ajayan, P. M. Large-scale synthesis of carbon nanotubes. *Nature* **358,** 220–222 (1992).
28. Bonard, J. M. *et al.* Purification and size-selection of carbon nanotubes. *Adv. Mater.* **9,** 827–831 (1997).


**Acknowledgements.** We thank H.-W. Fink, M. Henny, T. Hoss, M. Krüger, C. Terrier and V. Thommen for contributions. This work was supported by the Swiss National Science Foundation.

Correspondence and requests for materials should be addressed to C.S. (e-mail: Schonenberg@ubaclu.unibas.ch).

# Spontaneous chaotic granular mixing

**Troy Shinbrot, Albert Alexander & Fernando J. Muzzio**

*Pharmaceutical Engineering Program, Department of Chemical and Biochemical Engineering, Rutgers University, Piscataway, New Jersey 08854, USA*

**There are several types of instabilities in fluid mechanics that lead to spontaneous chaotic mixing and intricate patterns. Classical examples include the Kelvin–Helmholtz instability[1,2] in shear layers, the instability of Taylor–Couette flow between rotating cylinders[3,4] and the Rayleigh-Bénard instability in thermal convection[5]. More recently, a variety of two- and three-dimensional chaotic mixing phenomena have been observed in other geometries[6–9]. Mixing in granular flows[10,11], unlike that in stirred fluids, is thought to be diffusive—although periodic forcing has been used to enhance granular mixing[12,13], spontaneous chaotic granular mixing has not previously been reported. Here we report the observation of chaotic granular mixing patterns in simple cylindrical tumblers partially filled with fine grains. The patterns form spontaneously when sufficiently fine grains (≲300 μm diameter) are blended. We identify the mechanism by which the chaotic patterns are produced: a periodic stick–slip behaviour occurs in the shear layer separating static and flowing regions of grains. This causes weakly cohesive grains to mix at rates over-**